Structure, thermoelectric and electrical properties of bismuth-manganese oxide prepared by mechanochemical method

M.M. El-Desoky (mmdesoky@gmail.com)
Faculty of Petroleum and Mining Engineering, Suez University

Ahmed E. Hannora
National Research Institute of Astronomy and Geophysics (NRIAG)

Shereef A. Fareed
National Research Institute of Astronomy and Geophysics (NRIAG)

Makram Ibrahim
Assiut University

A M. Ali
Suez University

Research Article

Keywords: Bismuth manganese oxide, Mechanochemical technique, Amorphization, electrical conductivity

Posted Date: June 9th, 2021

DOI: https://doi.org/10.21203/rs.3.rs-598836/v1

Structure, thermoelectric and electrical properties of bismuth-manganese oxide prepared by mechanochemical method

Ahmed E. Hannora[1], Shereef A. Fareed[2], Makram Ibrahim[2], A M. Ali[3] M. M. El-*Desoky*[4]

1. Department of Sciences and Engineering Mathematics, Faculty of Petroleum and Mining Engineering, Suez University, Suez 4351, Egypt.

2.National Research Institute of Astronomy and Geophysics (NRIAG), Helwan 11421, Cairo, Egypt.

3.Department of Physics, Faculty of Science, Assiut University, Assiut 71516, Egypt.

4.Department of Physics, Faculty of Science, Suez University, Suez 43518, Egypt.

Abstract

Production of nanomaterials by mechanochemical synthesis is one of the important modern methods in new technology. Mechanochemical technique followed by heat treatment has been used to produce bismuth-manganese oxide from bismuth oxide and manganese dioxide. X-Ray Diffraction (XRD) analysis is conducted evaluate the structure changes during the mechanochemical process. Structure transformation from crystalline to complete amorphous phase was observed after short time of milling. The amorphization mechanism and reaction kinetics are examined in the light of the processing parameters and materials composition. Interdiffusion and distraction of the long rang order structure are the proposed mechanisms for amorphization. Bismuth manganese oxide phase with chemical formula $Bi_2Mn_4O_{10}$ was formed after heat treatment at 1073 K. $Bi_2Mn_4O_{10}$ partially decomposed to γ-$Bi_{12.8}O_{19.2}$ and α-Mn_2O_3. Crystallite size (47.6 - 102.4 nm) of the formed phases after heat treatment is significantly affecting the electrical properties. Thermoelectric power (***S***) of present samples was reported and the fraction C of reduced transition metal ions was calculated. The manganese ions concentration N were calculated and found to be increasing from 1.11 $X10^{22}$ cm^{-3} to 1.38 $X10^{22}$ cm^{-3}, while the average distance between manganese ions R increased from 0.623nm to 0.647nm. The hopping carrier mobility (μ) of the prepared samples was also calculated at fixed temperature. From studying the conduction mechanism, the present work was found to agree with non-adiabatic process of small polaron hopping.

Keywords

Bismuth manganese oxide; Mechanochemical technique; Amorphization, electrical conductivity.

1. Introduction

The combinational properties of multiferroic materials are considered as a main key for the importance of their widely found applications such as energy transducers [1] and battery electrodes [2]. Recently, Bi_2O_3-MnO_2 nanocomposites have been examined as electrode for supercapacitors [3]. Also, bismuth manganese oxide like $Bi_2Mn_4O_{10}$ can be used as catalysts for methane. The results showed that samples containing small amount of bismuth oxide with bismuth manganese oxide enhance catalytic activity [4]. Single-phase of $BiMnO_3$ was prepared in high energetic ball mill by mechanochemical synthesis method from Bi_2O_3 and Mn_2O_3 powder [5]. The perovskite $BiMnO_3$ phase obtained was formed after amorphization of the constituent materials [6]. The preparation of perovskite $BiMnO_3$ by solid-state reaction required high pressure and high temperature [7, 8]. $Bi_2Mn_4O_{10}$ single crystals are formed in the temperature range from 1173 K to 1223 K according to $Bi_2O_3 + 2\ Mn_2O_3 + 0.5\ O_2 \rightarrow Bi_2Mn_4O_{10}$. The orthorhombic $Bi_2Mn_4O_{10}$ belongs to a group of mullite-type compounds which have multiferroic properties at low temperatures [9]. Mechanochemical process is one of the common methods to produce nanocrystalline and/or amorphous phases. During the process repeated welding, fracturing and rewelding of powder particles are observed. The powder particles during milling trapped between the colliding balls undergo deformation and/or fracture processes [10-12].

Multiferroic materials have a magneto-electric behavior and exhibited ferro/antiferromagnetic and ferroelectric properties at the same time [13]. Generally, the manganite perovskite is one of the promising multiferroic materials due to its giant magneto-resistance. In this study, bismuth- based oxides with perovskite structure is selected as one of the extensively studied multiferroic compounds in the last decades. The cubic unit cell of the perovskite structure (ABO_3) is distorted into an orthorhombic structure. Multiferroic bismuth manganite materials such as $Bi_2Mn_4O_{10}$ and $BiMn_2O_5$ crystalizes in orthorhombic space group (Pbam) with two sites octahedral and pyramidal [14-16]. The unpaired electrons and the orbital ordering of Manganese cations are responsible for the coexistence of both ferromagnetic and ferroelectric properties [14]. The Curie temperature of the bismuth Manganite has value about 105 K and it exhibit ferroelectricity at the same time after Tc = 100 K [17, 18]. Bismuth Manganite materials can be prepared by different methods such as sol-gel combustion method or high energy ball milling of the constituent oxides [5]. Preparation using mechanochemical synthesis usually refers to solid-state reactions and can be used to prepare related compounds such as $Bi_2Mn_4O_{10}$ which is formed directly in highly activated nano-sized particles after only 240 minutes of high energetic milling [5].

The conductivity in nanostructure materials that contain large amounts transition metal ions (TMO) is described by small polaron hopping (SPH) mechanism between such ions [19, 20]. The carrier concentration (C) is related to the concentration of TMO in multivalence states [21-24]. The thermoelectric power or Seebeck coefficient (S) of the nanostructured materials that contain large amounts of (TMO) is great, which is required for many applications. Generally, Heike's formula [21] can be applied to evaluate the S and C values. In this study we focused on the structure, D.C. electrical conductivity and Seebeck coefficient of the resultant mixed oxides. The present work intends to examine the effect of mechanical milling process on Bi_2O_3 and MnO_2. The electrical properties of the produced samples were measured at different annealing time.

2. Experimental

High purity oxides of bismuth (Bi_2O_3) and manganese (MnO_2) (Aldrich 99%) were mixed using a stainless-steel vertical ball mill attritor with 500 r/m for different milling time. The prepared samples were pressed at 5 tons into a pellet with 12mm diameter using a uniaxial press. The pressed powder samples were heat treated at 873 K for 2h then calcining at 1073 K for 5h in open atmosphere. The X-ray diffraction patterns of the milled powder samples and heat treated were characterized using "SIEMENS D5000" X-ray Diffractometer with target CuKα radiation. Transmission Electron Microscope (TEM) using "JEM 2100 HRT" was carried out for the samples with 10h and 50h of milling to investigate their structure. The experimental density for the heat-treated samples was measured using Archimedes principle in order to calculate the other needed parameters in this study. As shown in Fig. 1 we investigate the D.C. electrical behavior of the samples, the temperature dependent-D.C. conductivity was calculated from the measured resistance using "Keithley 197" multi-meter. K-type thermocouple connected to a digital thermometer was used to measure the temperature inside non-inductive controllable electric furnace. The thermoelectric power or Seebeck coefficient was measured using the setup in Fig. 2 where two identical heaters with their accompanying K-type digital thermometers used to arise the temperature at the two sample's surfaces with difference ΔT, the induced voltage measured by "Agilent 34401A" multi-meter.

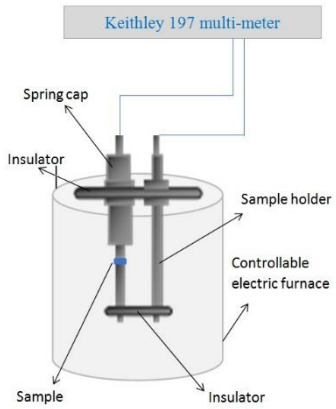

Fig. 1: D.C. conductivity measurement setup

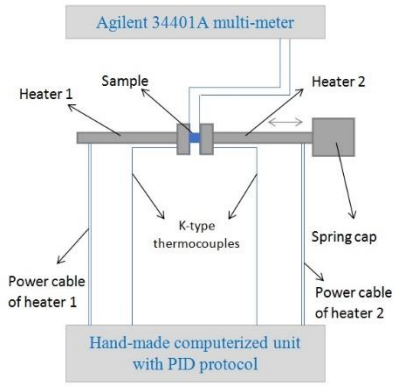

Fig. 2: Thermoelectric power measurement setup

3. Results and discussion

3.1 Structure

Figure 3 shows XRD patterns of mechanically treated $MnO_2 - Bi_2O_3$ system for different time. After one hour of treatment sharp crystalline peaks intensity decreases. The XRD peaks show significant broad due to crystallite size reduction and micro-strain increasing. This broadening behavior could indicate the starting of amorphization. After 10h of treatment all crystalline peaks mostly disappeared and hallow pattern tendency is observed. With increasing milling time up to 30h complete amorphization of the sample was observed. The milling time extended to 50h examining the recrystallization phenomenon. As shown in XRD there is no tendency for recrystallization appeared. The amorphization is controlled by diffusion; the faster transformation rate is related to the higher diffusion rate. During mechanical treatment, the exact nature of the stress acting process is rather complex. Since the extension of solubility limit is observed with milling, a dominant stress at atomic level expected. This type of external stress would be expected to accelerate the amount amorphization in the structure.

The crystallite size (D) and micro-strains (ε) of the mechanical milled sample can be estimated by using the full width at half maximum of the major peaks (β). Hall-Williamson relation was used to separate these factors:

$$\beta \cos\theta = \frac{K\lambda}{D} + 4\varepsilon \sin\theta \qquad (1)$$

where (θ) is the Bragg angle, λ is the wavelength and K is the Scherrer constant (shape factor) usually from 0.8 to 1.

The micro-strains estimated by Hall-Williamson relation varied from 0.078 (%) to 0.210 (%) with crystallite size ranged from 47.6 nm to 102.4 nm. Usually, the amorphization reaction during mechanical treatment is related to the strain generated in the samples which enhance

destabilization of the crystal structure. The amorphization in this case occurs through the destruction of the long-rang structure to the short-rang order. Fig. 4 shows TEM image of the mechanically treated MnO_2 – Bi_2O_3 powder after 10h and 50h of milling. Fine structure with laminar feature was observed for the 10h ball milled sample due to repeated impact process. The electron diffraction pattern of 10h milled sample with spot confirms fine structure formation while that of 50h sample shows completely amorphous nature. Halo is formed around the bright center spot where the electrons are scattered randomly by the short-rang order amorphous structure of specimen. Amorphous bismuth manganese oxides investigated as intercalation hosts for rechargeable lithium batteries [22].

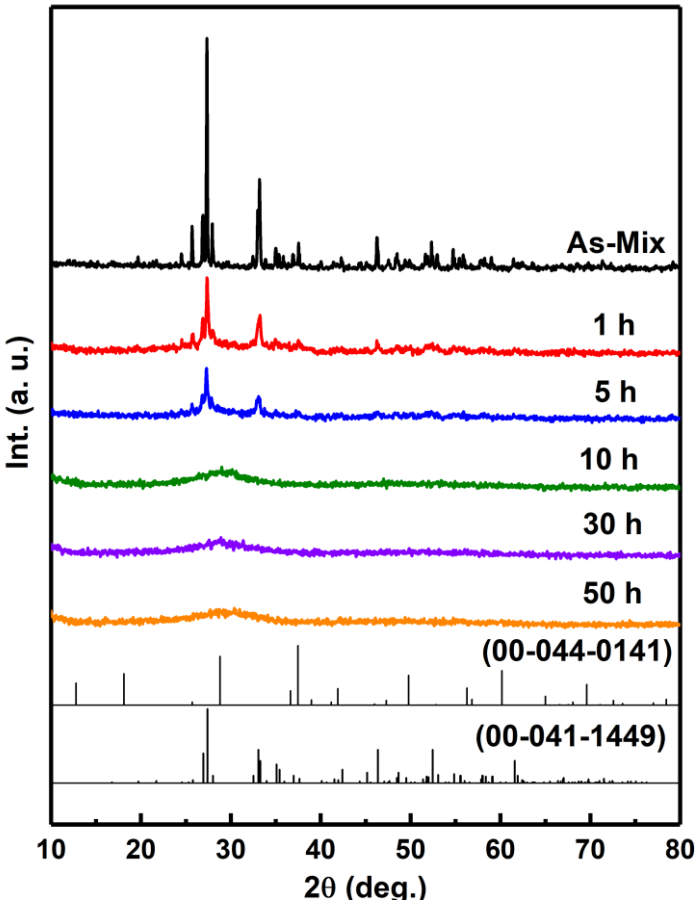

Fig. 3. XRD patterns of mechanically treated MnO_2 – Bi_2O_3 for different time

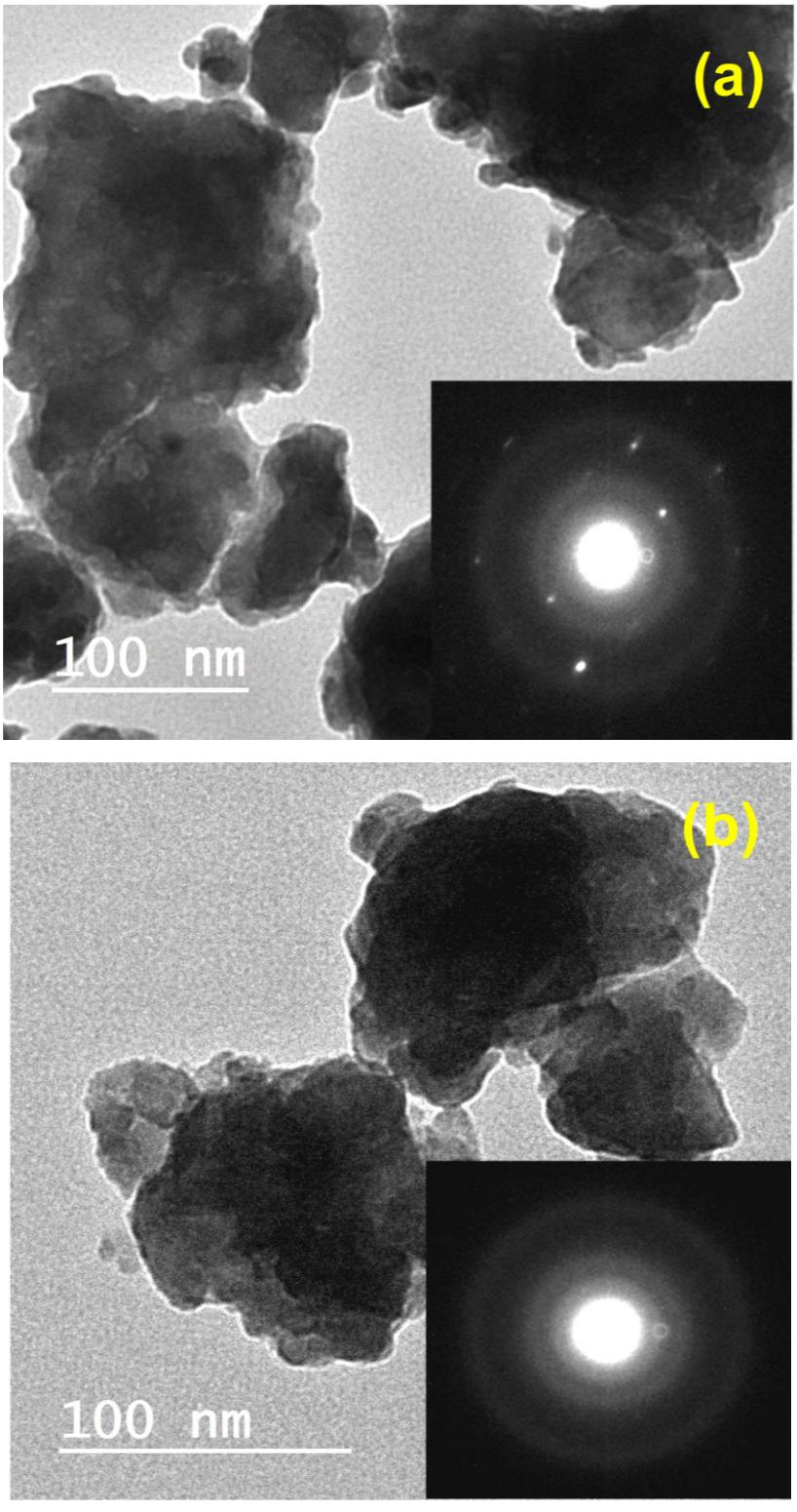

Fig. 4. TEM of 10h (a) and 50h (b) of mechanically treated $MnO_2 - Bi_2O_3$

Although, preparation of perovskite $BiMnO_3$ was successfully observed by high energy planetary ball mill [6]. Unfortunately, preparation of such perovskite by vertical ball mill (attritor) technique is not possible. This result could be due to the ball mill energy required is not

sufficient. Also, it is reported, preparation of perovskite $BiMnO_3$ by solid-state reaction required high pressure (6 GPa) and high temperature (1173 K) [7, 8].

Figure 5 shows XRD patterns of heat-treated mechanically milled $MnO_2 - Bi_2O_3$ samples at different time. Bismuth manganese oxide phase with chemical formulas $Bi_2Mn_4O_{10}$ was formed after 5h of heat-treatment at 1073 K. It is obvious that; after 10h of milling plus heat treatment mechano-chemical reaction take place resulting orthorhombic $Bi_2Mn_4O_{10}$ (01-074-1096) with space group Pbam (No. 55). The orthorhombic $Bi_2Mn_4O_{10}$ formed phase show (001) preferred orientation with heat treated one- and five-hours milling samples. The heat treatment of ball milled 30h and 50h samples revealed small amount of tetragonal Mn_3O_4 phase with space group I41/amd (No. 141). As expected, the orthorhombic phase decreases with increasing milling time at the same heat treatment temperature. It is concluded that, $Bi_2Mn_4O_{10}$ decomposes to α-Bi_2O_3 and α-Mn_2O_3 [4]. Also, $BiMn_2O_5$ has a structure, which contains octahedrally coordinated Mn^{4+}ions and Mn^{3+}ions located in square pyramids [23].

In the present work, the decomposition clearly observed with 50h milled sample where cubic system with space group I23 (No. 197) γ-$Bi_{12.8}O_{19.2}$ (01-081-0563) and tetragonal system with space group I41/amd (No. 141) α-Mn_2O_3 are formed. Table 1 shows quantitative analysis, crystallite size and micro-strain of the heat-treated samples. Recently, $Bi_2Mn_4O_{10}$ compound has been investigated as an anode material for advanced Li-ion battery systems [24, 25]. Variation of lattice parameters as a function of milling time at the same heat treatment temperature (1073 K for 5 hours) is illustrated in Table 2.

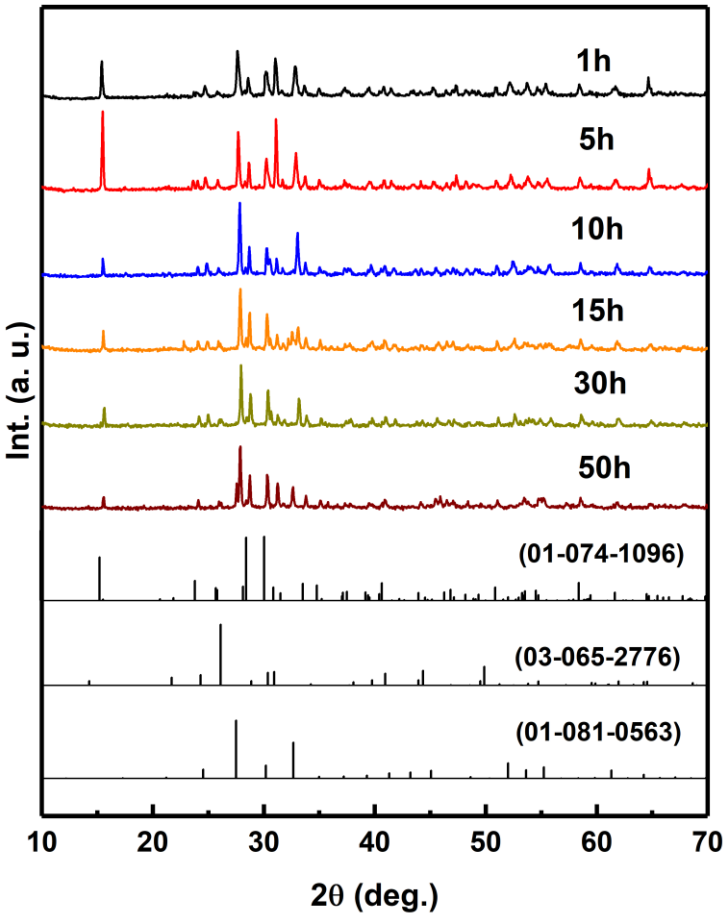

Fig. 5. XRD patterns of ball milled $MnO_2 - Bi_2O_3$ for different time heat-treated at 1073 K

Table 1: Quantitative analysis, crystallite size and micro-strain of heat-treated samples at 1073 K for 5 hours

Mechanical treatment time (hours)	1	5	10	15	30	50
$Bi_2Mn_4O_{10}$ (%)	81	88	66	68	36	39
α-Mn_3O_4 (%)	7	7	9	8	10	11
γ-$Bi_{12.8}O_{19.2}$ (%)	12	5	25	24	54	50
Average Crystallite size D(nm)	47.6	58.1	110.3	95.7	94.6	102.4
Micro-Strain (%)	0.078	0.11	0.21	0.136	0.146	0.21

Table 2: Variation of lattice parameters as a function of milling time at constant heat treatment temperature (1073 K for 5 hours)

Phase	a	b	c	Note
$Bi_2Mn_4O_{10}$	7.52	8.53	5.77	1h
	7.51	8.53	5.77	5h
	7.54	8.53	5.69	10h
	7.46	8.53	5.76	30h
	7.48	8.53	5.76	50h
	7.54	8.53	5.77	01-074-1096
γ-$Bi_{12.8}O_{19.2}$	10.19			1h
	10.18			5h
	10.14			10h
	10.09			30h
	10.26			50h
	10.23			01-081-0563

3.2 Thermoelectric power and D.C. Conductivity

Thermoelectric power was measured versus temperature for the prepared samples with milling time 10h, 30h and 50h. Fig. 6 shows the Seebeck coefficient (S) variation for each sample, the value decreased from -108 µV/K at 10h milling time to -128 µV/K at 30h and then increased to be -88 µV/K at 50h.

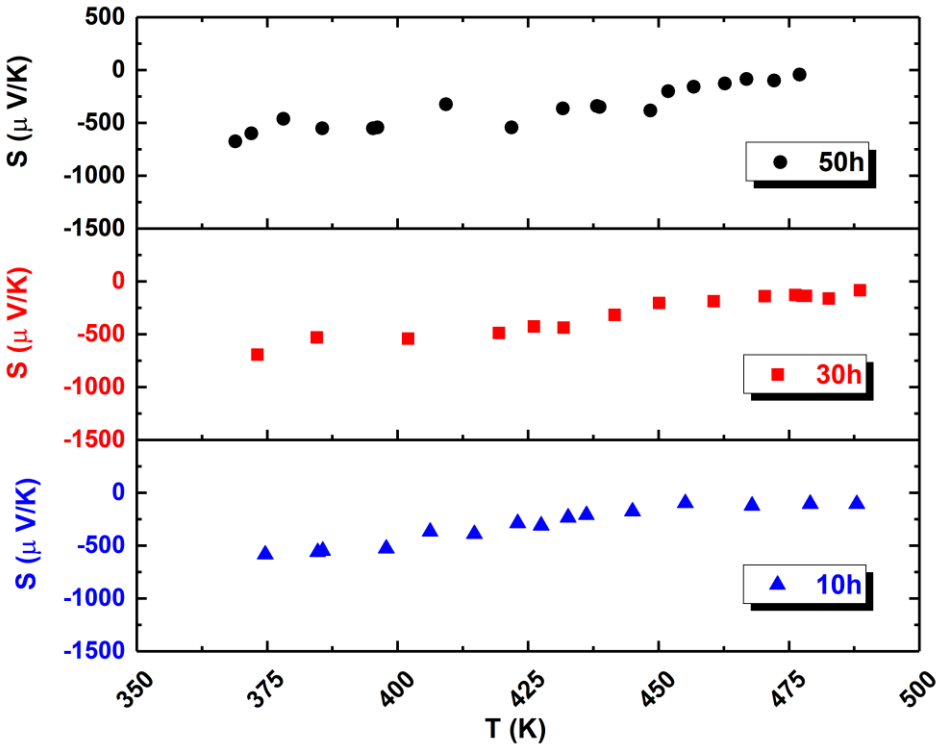

Fig. 6. Seebeck coefficient of the sample at different milling time, 10h at (a), 30h at (b) and 50h at (c)

The negative value of Seebeck coefficient indicates n-type conductivity. The obvious increase of |S| with increasing temperature (300K – 480K) is backed to the small-polaron conduction mechanism with reducing the concentration of the Mn^{3+} ions [26]. Thermopower (Seebeck coefficient) was used to determine the concentration ratio (C) from temperature independent Heike equation as:

$$S = \frac{k}{e}\left[\ln\left(\frac{C}{1-C}\right) + A\right] \quad (2)$$

For small polaron hopping conductors, A is neglected. The ratio of the concentration of reduced transition metal increases from 0.022 to 0.027.

In order to examine electrical properties, D.C conductivity (σ) and reciprocal of temperature (1/T) of the present samples have been showed in Fig. 8. As shown, the Arrhenius formula by Mott can be used to describe the behavior of D.C conductivity:

$$\sigma = \sigma_0 exp\,(-W/kT) \quad (3)$$

where w is the activation energy, k is Boltzmann constant and σ_0 is a pre-exponential factor. As illustrated in Fig. 7, the logarithmic D.C conductivity variation against the reciprocal of temperature for the heat-treated samples at 1073 K for five hours. The behavior represents the Arrhenius plot between 300K and 425K. The deviation from linearity (at high temperature regime) occurred around $\theta_D/2$ (353-369K depending on milling time). The obtained values of Debye temperature θ_D at the end of the linear dependency of the D.C. conductivity were varied from 706K to 770K as listed in Table 3. The linearity after this point (706K) is not best preserved which indicates small polaron hopping (SPH) [27].

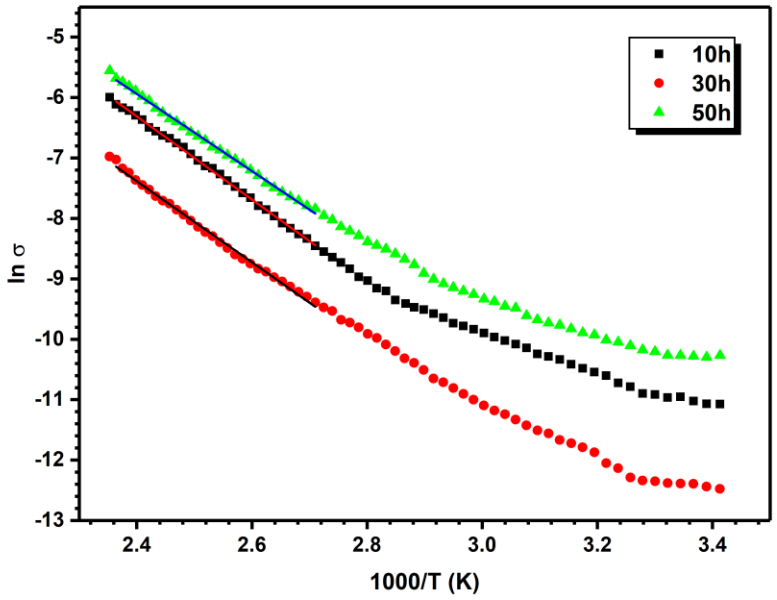

Fig. 7. dc conductivity of ball milled $MnO_2 – Bi_2O_3$ for different time heat-treated at 1073 K for five hours.

Thermoelectric power and conductivity measurements confirming presence of a small number of electrons, due to incomplete oxidation of the sample. It is reported [28], the perfectly stoichiometric manganite $CaMnO_3$ should not contain Mn^{3+} cations. In the n-type manganite, Mn^{4+} ions offer available sites for charge carriers, take into account the spin state of the Mn^{4+} ions. With increasing temperature concentration of Mn^{3+} disproportionation increases which influencing charge carriers through forming Mn^{2+} and Mn^{4+} from $2Mn^{3+}$. Oxygen addition/removal from the structure of the manganite plays significant rule in the electrical properties. The conduction through small-polaron transport between Mn^{3+} and Mn^{4+} ions[28]. From the above results of |S| and σ, the samples can be used as thermoelectric transducers due to the large values of |S| at room temperature, the best sample is that with 50h milling because its own the largest values of both Seebeck coefficient |S| and D.C. conductivity.

Activation energy value of 0.4 eV was observed for $Bi_{12}MnO_{20}–BiMn_2O_5$ compound with small polaron mechanism of electric conductivity and values of disordered $Bi_{12}MnO_{20}–BiMn_2O_5$–Fe ceramics were varied in the range of 0.22–0.37 eV [23]. $BiMnO_3$ has activation energy value of 0.51 eV [29]. The experimentally measured activation energy for electrical conductivity in stoichiometric bismuth manganite $BiMnO_3$ yields a comparable value 0.26 eV [30]. The present work activation energy values varied in the range of 0.55 to 0.63 eV depends on the milling time. The formed phases and/or crystallite size significantly affecting the Mn–O–Mn bond length and bond angle. The deformation of unit cell, see Table 2, resulted from the mechanical treatment

customized the overlapping of O (p-orbitals) and Mn (d-orbitals). Through double exchange mechanism Mn^{3+}–O–Mn^{4+} electron-hopping conduction allowed.

In non-adiabatic approximation, the DC conductivity for the hopping polarons proposed by Austin and Mott [31-33]:

$$\sigma = C(1-C).\frac{\nu_0 N e^2 R^2}{kT} \exp(-2\alpha R) \exp\left(-\frac{W}{kT}\right) \quad (4)$$

For adiabatic approximation, the term exp(-αR) is neglected and the conductivity is given by:

$$\sigma = C(1-C).\frac{\nu_0 N e^2 R^2}{kT} \exp\left(-\frac{W}{kT}\right) \quad (5)$$

N is the number of transition metal ion sites per unit volume (transition metal ion density) which estimated by:

$$N = \rho N_A \left[\frac{\text{Mole percent of composition}}{\text{Average molecular weight of compoition}}\right] \quad (6)$$

N_A is the Avogadro's number and ρ is the sample density which experimentally measured from Archimedes principle using Toluene liquid as an immersing medium with density 0.8669 g/cm3.

α is the electron-wave function decay constant (tunneling factor), C is the ratio of the ion concentration in the low valence state to the total concentration of the transition metal ions, R is average Hopping distance and ν_o is the optical phonon frequency. The activation energy W can be described as:

$$W = W_D \quad \text{for } T < \frac{\theta_D}{4} \quad (7)$$

$$W = W_H + \left(\frac{W_D}{2}\right) \quad \text{for } T > \frac{\theta_D}{2} \quad (8)$$

where W_H is the polaron hopping energy and W_D is the disorder energy (with typical value = 0.1 eV) [34]. By using Debye temperature θ_D and Planck constant h, the optical phonon frequency ν_o can be calculated as [35, 36]:

$$\nu_o = \frac{k\,\theta_D}{h} \quad (9)$$

The average distance between manganese (R) is related to number of sites per unit volume by the relation:

$$R = \left(\frac{4\pi N}{3}\right)^{-\frac{1}{3}} \quad (10)$$

The calculated parameters; molar volume (V_m), molar concentration (N), mean distance between ions (R) and the optical phonon frequency (ν_0) were listed in Table (3). The modulus of

Seebeck coefficient |S| increased from 108 μV/K to 128 μV/K due to mean distance between manganese ions "R" and the crystallite size "D" variation.

Table 3: some physical properties of the prepared samples

Milling time (h)	**10**	**30**	**50**
Debye Temperature θ_D(K)	706	770	738
Molar Volume V_m(cm^3/mol)	34.80	34.68	38.98
Electric Conductivity σ (Sm^{-1})	0.00095	0.00033	0.0015
Activation Energy W(eV)	0.587	0.625	0.554
Density ρ (gm/cm^3)	8.960	8.990	8.000
Number of Vanadium Ions N ($\times 10^{22}$) (cm^{-3})	1.7305	1.7363	1.5451
Average distance between manganese R(nm)	0.623	0.622	0.647
Optical Phonon Frequency ν_0 ($\times 10^{13}$)	0.735	0.802	0.766

At a fixed experimental temperature, it is easy to estimate the nature of polaron hopping, adiabatic or non-adiabatic by plotting activation energy against logarithm of the conductivity. By calculating the slope and interception as illustrated in Fig. (8 a and b), the resultant temperature is T=539.6 K. According to the above results, the conduction is due to non-adiabatic small polaron hopping of electrons because there is a big difference between the estimated temperature and the selected measurement temperature (401K). Also, the effect of milling time on the pre-exponential factors (σ_o) obtained from the straight line fitting the data. The decrease of pre-exponential factors with milling time confirming again the non-adiabatic mechanism of the polaron hopping.

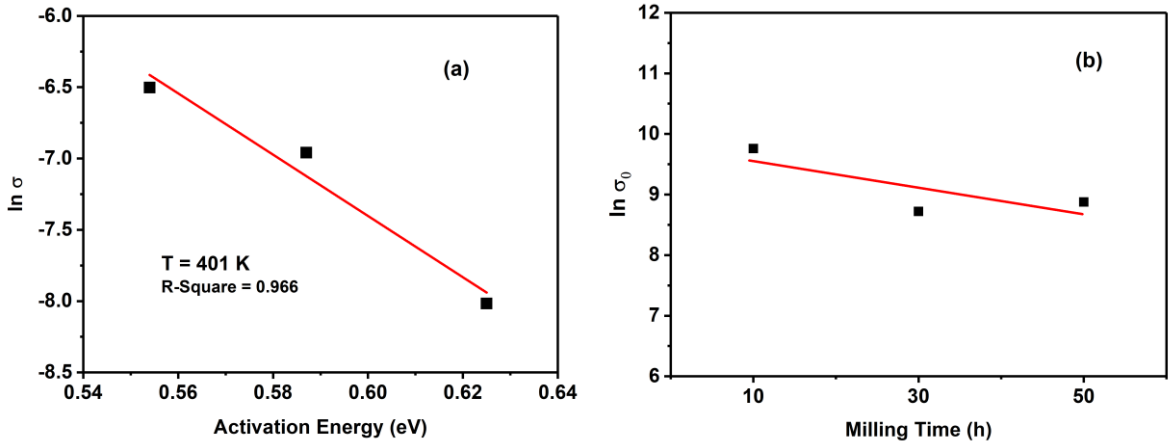

Fig. 8: (a) samples logarithmic D.C conductivity variation with activation energy at 401K, (b) effect of milling time on the pre-exponential factors

The density of state at the Fermi level $N(E_F)$ is estimated from the following expression:

$$N(E_F) = ¾\ \pi R^3 W \qquad (11)$$

The values of $N(E_F)$ are listed in Table 4 and acceptable for the localized states.

The polaron radius (r_p) can be calculated from R using the following relation [37]

$$r_p = \left(\frac{\pi}{6}\right)^{\frac{1}{3}} . \frac{R}{2} \qquad (12)$$

then, the value r_p used to obtain the hopping energy W_H using the formula:

$$W_H = \left(\frac{e^2}{4\varepsilon_p}\right)\left(\frac{1}{r_p} - \frac{1}{R}\right) \qquad (13)$$

$$\frac{1}{\varepsilon_p} = \frac{1}{\varepsilon_\infty} - \frac{1}{\varepsilon_s} \qquad (14)$$

where ε_p *is* effective dielectric constant , ε_∞ is the static dielectric constant measured at high frequency (1MHz) and ε_s is the optical dielectric constant. The values of r_p, ε_p and W_H are listed in Table 4.

The bandwidth of polaron associated with the electron wave function overlapping on the near sites J can be calculated from using the following relation [37]

$$J \approx e^3[N(E_F)/(\varepsilon_o \varepsilon_p)^3]^{1/2} \qquad (15)$$

The values of bandwidth of polaron J are recorded in Table 4.

The small polaron coupling constant γ_p represents the interaction between polaron and electron

$$\gamma_P = \frac{2\, W_H}{h\, \nu_o} \qquad (16)$$

The calculated values of γ_p are 12.57–23.40 for the present samples. It is noticed that the value of $\gamma_p > 4$, this usually suggests a strong electron-phonon interaction[45] . The values of small polaron coupling constant γ_p are recorded in Table 4.

The charge carrier mobility (μ) in the non-adiabatic hopping regions is calculated using the formulas

$$\mu = \left(\frac{eR^2}{kT}\right)\left(\frac{1}{h}\right)\left(\frac{\pi}{4\, W_H kT}\right)^{1/2} J^2 \exp\ -\frac{W}{kT} \qquad (17)$$

The obtained carrier mobility by using parameters listed in Tables 3 and 4 at T= 401 K for the present samples. The calculated values of carrier mobility are found to be in the range 1.685 x 10^{-6} cm^2 V^{-1} s^{-1} to 2.689 x 10^{-6} cm^2 V^{-1} s^{-1}), which is << 0.01 indicating that the electrons are

localized mainly at manganese ions [34]. The values of hopping carrier mobility (μ) are registered in Table 4.

Table 4 polaron hopping parameters

Milling time (h)	10	30	50
W_D (eV)	0.00645	0.0505	0.0483
W_H(eV)	0.584	0.600	0.530
ϵ_P	56.2	28.7	27.8
r_p (nm)	0.251	0.251	0.261
J(eV)	0.236	0.630	0.661
$N(E_f)$ (cm^{-3}) $\times 10^{21}$	1.68	1.58	1.59
γ_p	12.57	22.61	23.40
μ (cm^2 V^{-1} S^{-1}) $\times 10^{-6}$	1.685	2.874	2.689

4. Conclusion

1. Amorphization of the prepared samples is observed to take please after 10h of mechanical milling in vertical ball mill attritor.
2. Bismuth manganese oxide $Bi_2Mn_4O_{10}$ was formed after heat-treatment.
3. Preparation of perovskite $BiMnO_3$ by vertical ball mill attritor technique unfortunately is not possible.
4. The conduction of the prepared samples is well-explained by Mott's small polaron theory, it is attributed to non-adiabatic hopping of small polaron (SPH)
5. The modulus value of Seebeck coefficient of the samples with 10h, 30h and 50h milling time is inversely proportional to the obtained crystallite size.
6. The hopping carrier mobility μ was investigated and found varying from 1.685 $x10^{-6}$ cm^2 V^{-1} S^{-1} to 2.689$x10^{-6}$ cm^2 V^{-1} S^{-1}.
7. The polaron radius r_p increase from 0.251nm to 0.261nm, while the density of states at the Fermi level $N(E_F)$ decreased from 1.68 $x10^{21}$ eV^{-1} cm^{-3} to 1.59 $x10^{21}$ eV^{-1} cm^{-3}.
8. The non-adiabatic nature of polaron hopping mechanism was established in different ways.
9. The sample with 50h milling time has the largest polaron radius and can be used as a thermoelectric transducer due to the large modulus value of Seebeck coefficient |S| and D.C. conductivity.

References:

[1] Z.S. D. Bochenek, Multiferroic materials for sensors, transducers and memory devices, Archives of Acoustics 33 (2008) 243-260

[2] H.Z. Z. Song, K. Feng, H. Wang, X. Li, H. Zhang $Bi_2Mn_4O_{10}$: a new mullite-type anode material for lithium-ion batteries, Dalton Transactions 47 (2018) 7739-7746.

[3] S.J.Z. J.J. Ma, Q.Y. Shan, S.F. Liu, Y.X. Zhang, F. Dong, H.D. Liu, Facile Synthesis of Flower-like (BiO)(2)CO_3@MnO_2 and Bi_2O_3@MnO_2 Nanocomposites for Supercapacitors, Electrochimica Acta 168 (2015) 97-103.

[4] I. Baidikova, H. Matralis, J. Naud, C. Papadopoulou, E.A. Mamedov, B. Delmon, Characterization of bismuth-manganese oxide catalysts for methane oxidative coupling, Applied Catalysis A: General 89(2) (1992) 169-182.

[5] S.Z.B. Z. Marinkovic, Z. Jaglic , M. Jagodic, L. Mancic, S. Bernik, A. Recnik, G. Brankovic, Structural and magnetic properties of nanocrystalline

bismuth manganite obtained by mechanochemical synthesis, J Nanopart Res 13 (2011) 3431–3439

[6] Z. Branković, Z.M. Stanojević, L. Mančić, V. Vukotić, S. Bernik, G. Branković, Multiferroic bismuth manganite prepared by mechanochemical synthesis, Journal of the European Ceramic Society 30(2) (2010) 277-281.

[7] Z.H. Chi, H. Yang, S.M. Feng, F.Y. Li, R.C. Yu, C.Q. Jin, Room-temperature ferroelectric polarization in multiferroic BiMnO3, Journal of Magnetism and Magnetic Materials 310(2, Part 2) (2007) e358-e360.

[8] Z.H. Chi, C.J. Xiao, S.M. Feng, F.Y. Li, C.Q. Jin, X.H. Wang, R.Z. Chen, L.T. Li, Manifestation of ferroelectromagnetism in multiferroic BiMnO3, Journal of Applied Physics 98(10) (2005) 103519.

[9] M. Burianek, T.F. Krenzel, M. Schmittner, J. Schreuer, R.X. Fischer, M. Mühlberg, G. Nénert, H. Schneider, T.M. Gesing, Single crystal growth and characterization of mullite-type Bi2Mn4O10, International Journal of Materials Research 103(4) (2012) 449-455.

[10] A.E. Hannora, Preparation of calcium manganese phosphate by mechanochemical synthesis of manganese and hydroxyapatite, Journal of the Australian Ceramic Society 55(3) (2019) 807-815.

[11] A.E. Hannora, S. Ataya, Structure and compression strength of hydroxyapatite/titania nanocomposites formed by high energy ball milling, Journal of alloys and compounds 658 (2016) 222-233.

[12] A. Hannora, A. Mamaeva, Z. Mansurov, X-ray investigation of Ti-doped hydroxyapatite coating by mechanical alloying, Surface Review and Letters 16(5) (2009) 781-786.

[13] O.J. S.N. Achary, A.K. Tyagi, Multiferroic Materials, Functional Materials (2012) 155-191.

[14] R.R. A. K. Kundu, V. Pralong, V. Gaignaert, B. Raveau, Magneto-transport and magneto-dielectric effects in Bi-based perovskite

manganites, J. Mater. Chem 18 (2008) 4280–4285

[15] L.K. F. Ziegler, H. Gibhardt, T. M. Gesing, M. M. Murshed, O. Sobolev, A. Piovano, GötzEckold, Characterization of Multiferroic $Bi_2Mn_4O_{10}$ by Dielectric and Neutron Spectroscopy, Phys. Status Solidi B 256 (2019) 1800668.

[16] J.T.A. Z. R. Kann, E. W. Hearn, S. U. Weber, K. D. Becker, H. Schneider, M. W. Lufaso, Mixed crystal formation and structural studies in the mullite-type system $Bi_2Fe_4O_9$–$Bi_2Mn_4O_{10}$, Journal of Solid State Chemistry 185 (2012) 62–71.

[17] A.A. Belik, Journal of Solid State Chemistry 246 (2017) 8-15

[18] M.H. S. Hanif, S. Riaz, S. Atiq, S. S. Hussain, S. Naseem, G. Murtaza, Structural, magnetic, dielectric and bonding properties of $BiMnO_3$ grown by co-precipitation technique, Results in Physics 7 (2017) 3190-3195

[19] V. Naresh, S. Buddhudu, Studies on Optical, Dielectric and Magnetic Properties of Mn2+, Fe3+ & Co2+ Ions Doped LFBCd Glasses, Ferroelectrics 437 (2012).

[20] L. Murawski, R. Barczyński, Dielectric relaxation in semiconducting oxide glasses, Journal of Non-crystalline Solids - J NON-CRYST SOLIDS 196 (1996) 275-279.

[21] R.W.U.E. R.R. Heikes, Thermoelectricity, Interscience, New York, (1961).
[22] J. Yang, T.B. Atwater, J.J. Xu, Improved cycling performance of bismuth-modified amorphous manganese oxides as cathodes for rechargeable lithium batteries, Journal of Power Sources 139(1) (2005) 274-278.
[23] A. Leonarska, M. Kądziołka-Gaweł, A.Z. Szeremeta, R. Bujakiewicz-Korońska, A. Kalvane, A. Molak, Electric relaxation and Mn3+/Mn4+ charge transfer in Fe-doped Bi12MnO20–BiMn2O5 structural self-composite, Journal of Materials Science 52(4) (2017) 2222-2231.
[24] J. Zhan, C.-f. Xu, Y.-y. Long, Q.-h. Li, Preparation and electrochemical performance of nitrogen-doped carbon-coated Bi2Mn4O10 anode materials for lithium-ion batteries, Transactions of Nonferrous Metals Society of China 30(8) (2020) 2188-2199.
[25] J. Zhan, Y. Long, Synthesis of Bi2Mn4O10 nanoparticles and its anode properties for LIB, Ceramics International 44(12) (2018) 14891-14895.
[26] E.I.K. I. A. Leonidov, M. V. Patrakeev, A. A. Markov, V. L. Kozhevnikov, Seebeck Coefficient of $Ca_{1-x}Pr_xMnO_{3-\delta}$ Paramagnetic Manganites, Inorganic Materials 53 (2017) 583-588
[27] M.S.A.-A. A. M. Al-Syadi, H. M. A. Hassan, M. M. El-Desoky, Grain size effects on the transport properties of $Li_3V_2(PO_4)_3$glass–ceramic nanocomposites for lithium cathode batteries, J Mater Sci. 27 (2016) 4074-4083.

[28] I.A. Leonidov, E.I. Konstantinova, M.V. Patrakeev, A.A. Markov, V.L. Kozhevnikov, Seebeck coefficient of Ca1–xPrxMnO3–δ paramagnetic manganites, Inorganic Materials 53(6) (2017) 583-588.

[29] M.S. Dar;, K.B. Akram, Evidence of Variable Range Hopping (VRH) and Exchange Interaction in Co-Doped Multiferroic $BiMnO_3$ Nanoparticles, J. Supercond. Nov. Magn 27(613–623) (2014).

[30] A. Molak, D.K. Mahato, A.Z. Szeremeta, Synthesis and characterization of electrical features of bismuth manganite and bismuth ferrite: effects of doping in cationic and anionic sublattice: Materials for applications, Prog. Cryst. Growth Charact. Mater. 64(1) (2018) 1-22.
[31] N.F.M. I.G. Austin, Polarons in crystalline and non-crystalline materials, Adv. Phys. 18(71) (1969) 41-102
[32] M.M.M. M. M. El-Desoky, M. S. Ayoub, M. A. Ahmed, Transport properties of Ba-doped $BiFeO_3$ multiferroic nanoparticles, J Mater Sci 26 (2015) 6793-6800

[33] N.F. Mott, Electrons in disordered structures, Adv. Phys 16 (1967) 49-144.
[34] A. Ghosh, B.K. Chaudhuri, DC conductivity of V_2O_5-Bi_2O_3 glasses, Journal of Non-Crystalline Solids 83(1) (1986) 151-161.
[35] D.A. H. Hirashima, T. Yoshida, Electrical Conductivity of PbO-P_2O_5-V_2O_5Glasses, J. Am. Ceram. Soc. 68 (1985) 486
[36] A.A.-H. A. Al-Shahrani, M. M. El-Desoky, Non-adiabatic small polaron hopping conduction in sodium borate tungstate glasses phys. stat. sol (a) 2 (2003) 378–387.[37] E.K.K. V. N. Bogomolov, YU. A. Firsov, Sov, Polaron nature of the current carriers in rutile TiO_2, phs. Solid state 9 (1968) 2502.

Figures

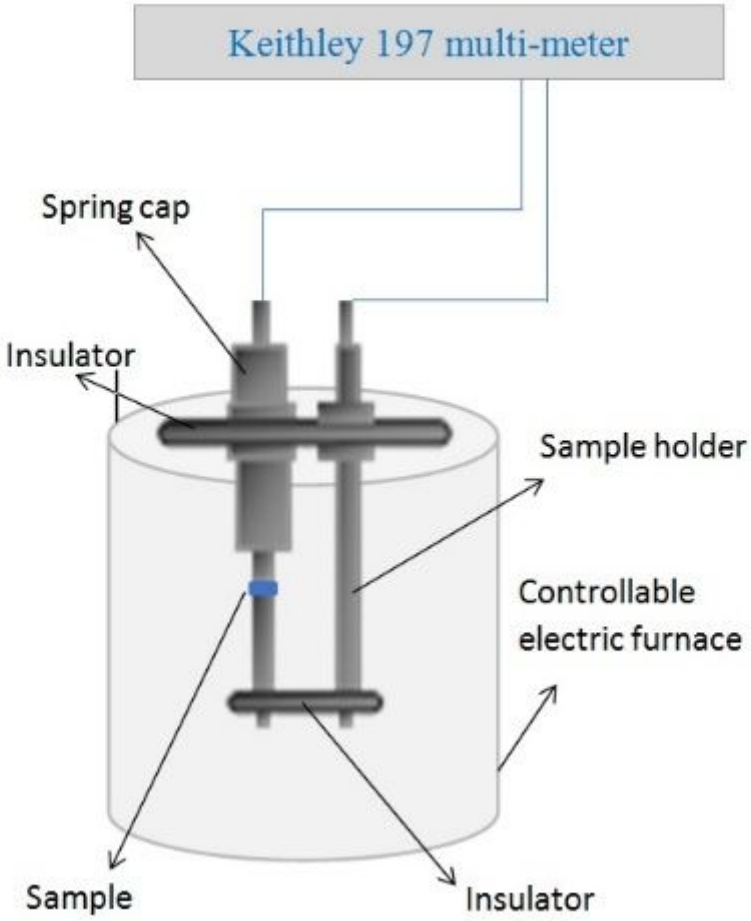

Figure 1

D.C. conductivity measurement setup

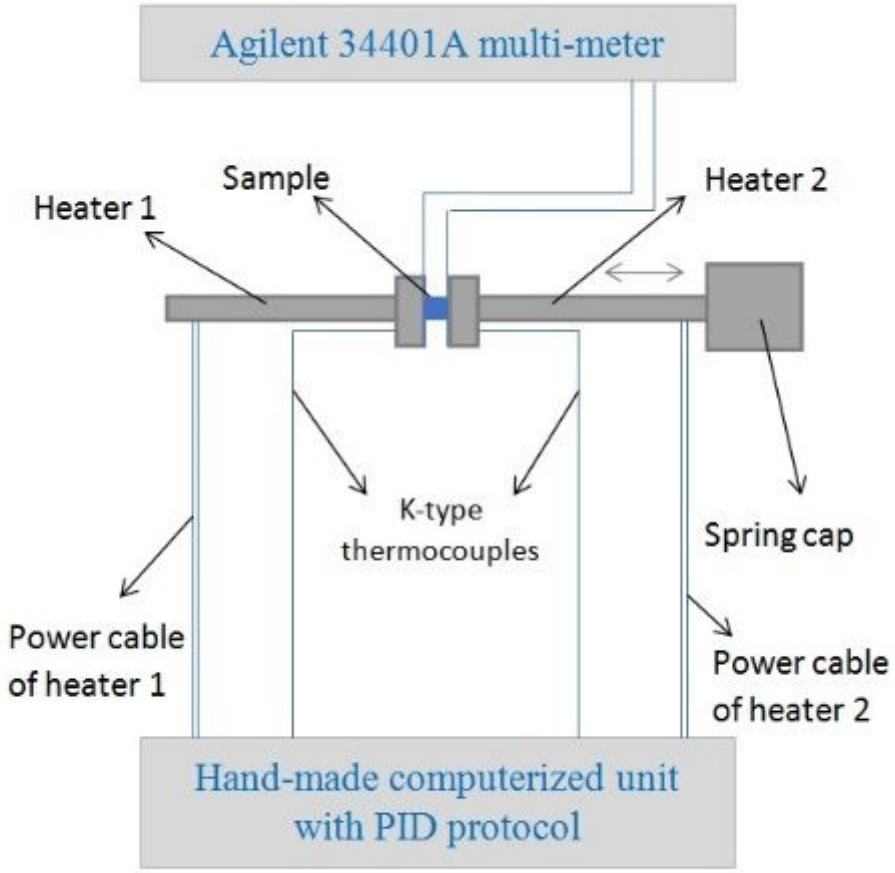

Figure 2

Thermoelectric power measurement setup

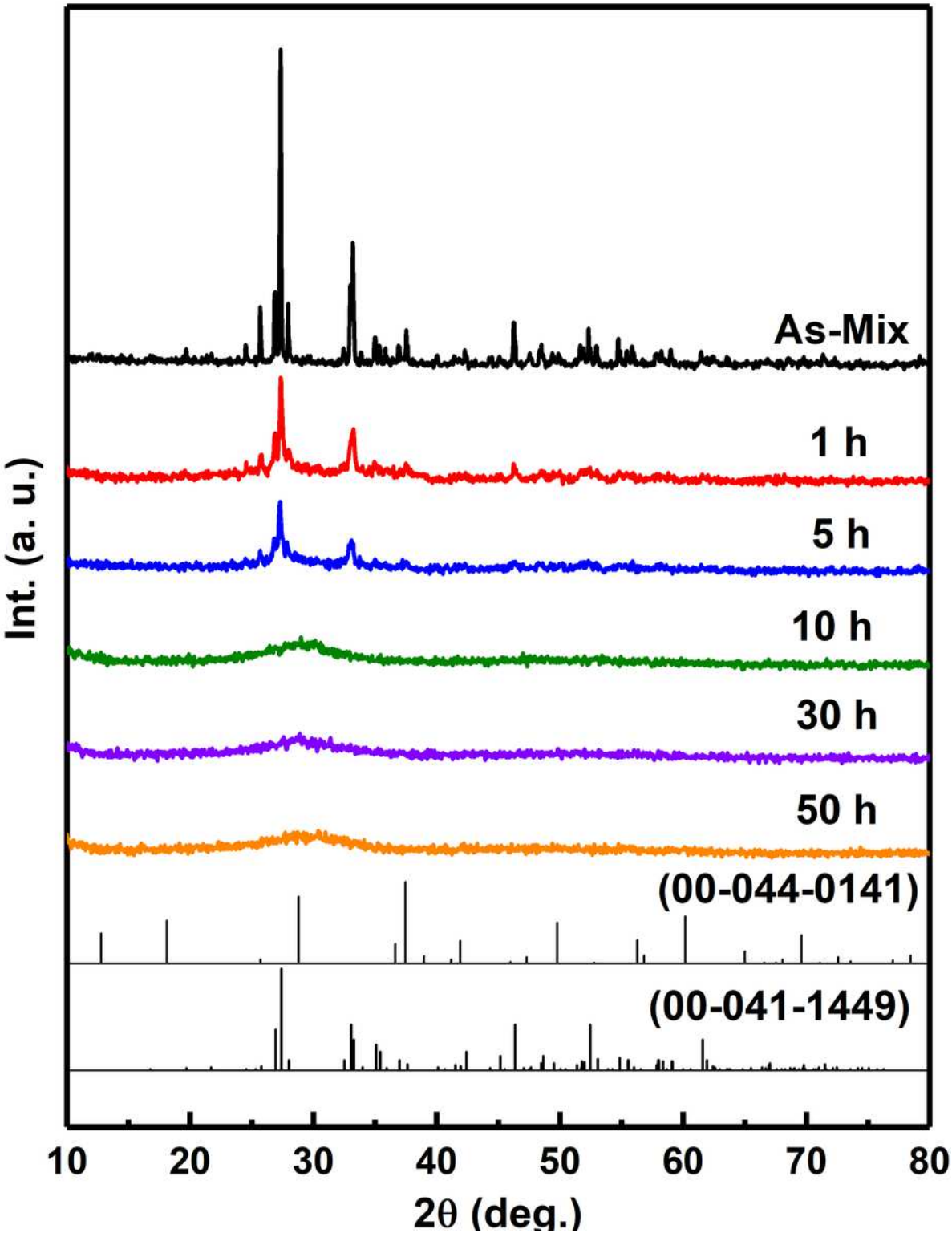

Figure 3

XRD patterns of mechanically treated MnO2 – Bi2O3 for different time

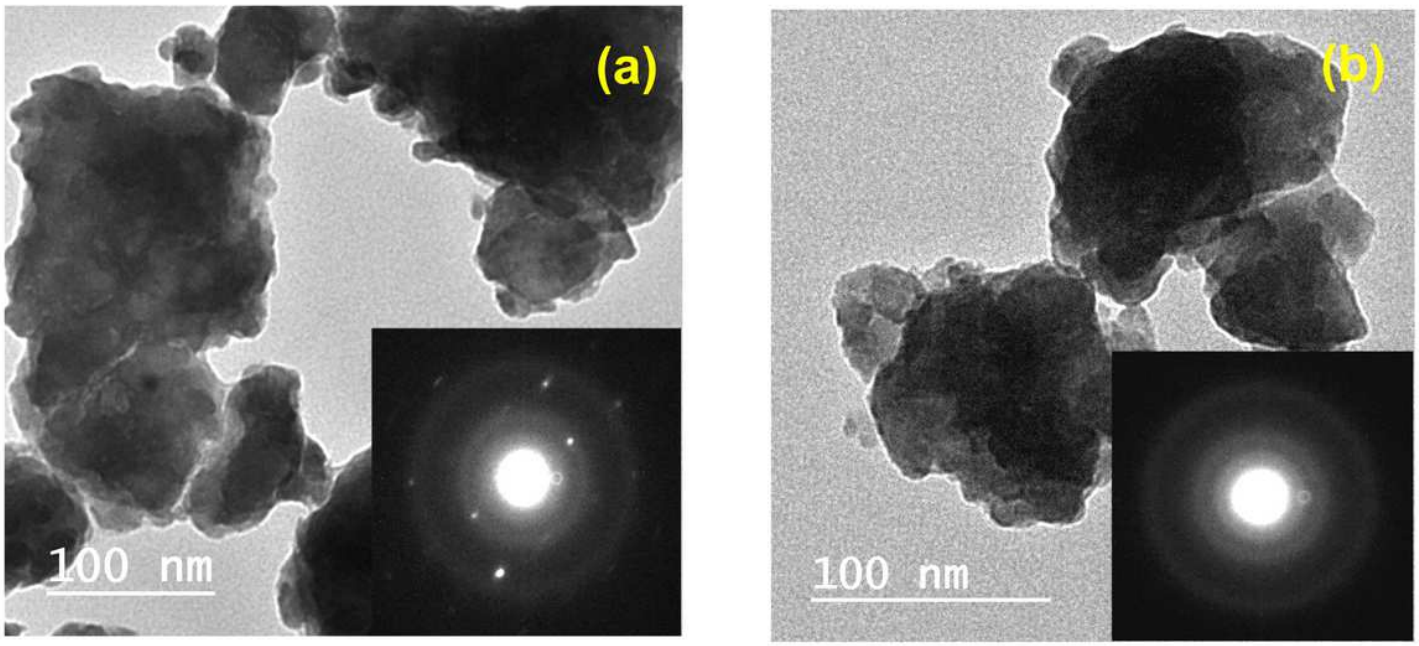

Figure 4

TEM of 10h (a) and 50h (b) of mechanically treated MnO2 Bi2O3

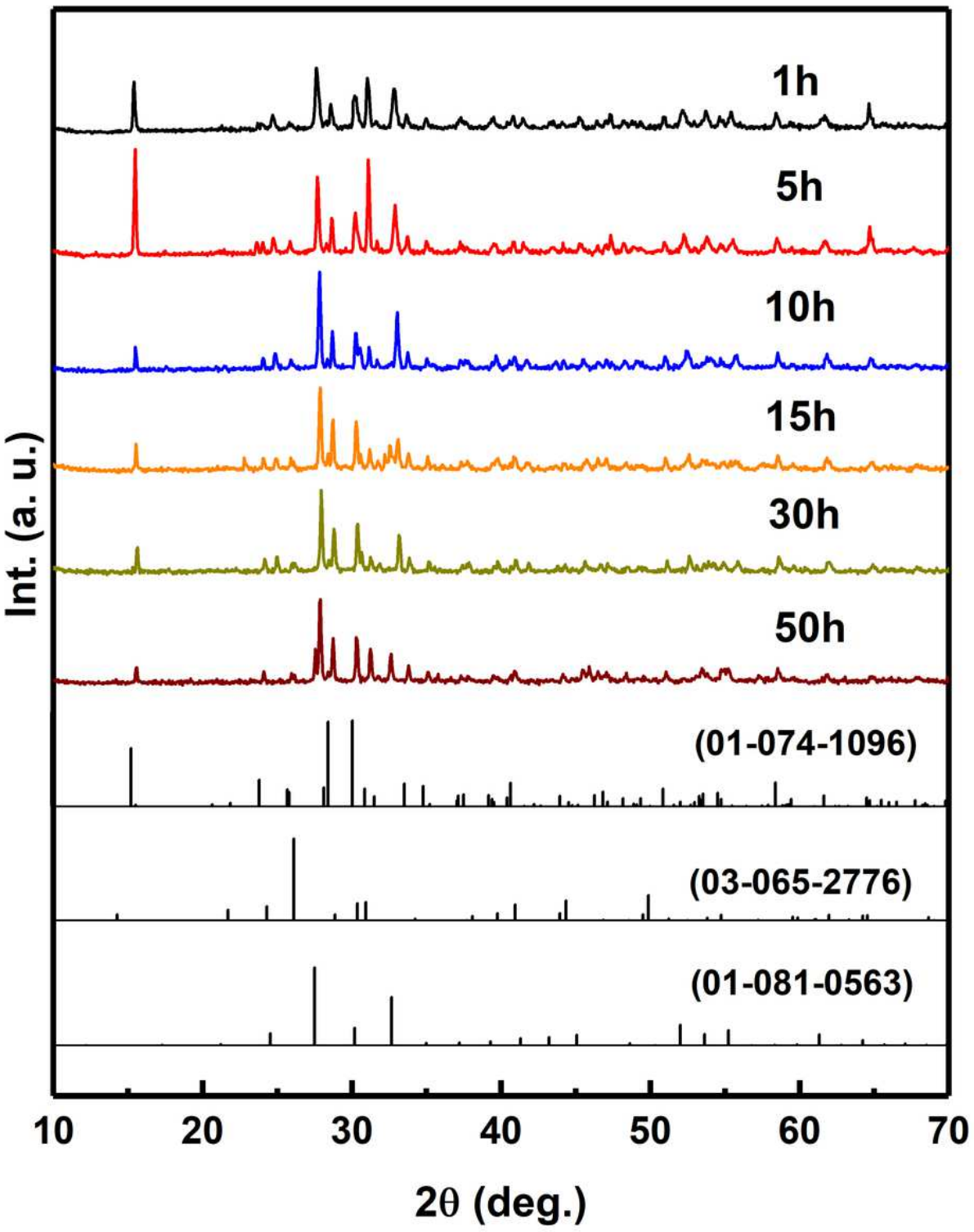

Figure 5

XRD patterns of ball milled MnO2 Bi2O3 for different time heat-treated at 1073 K

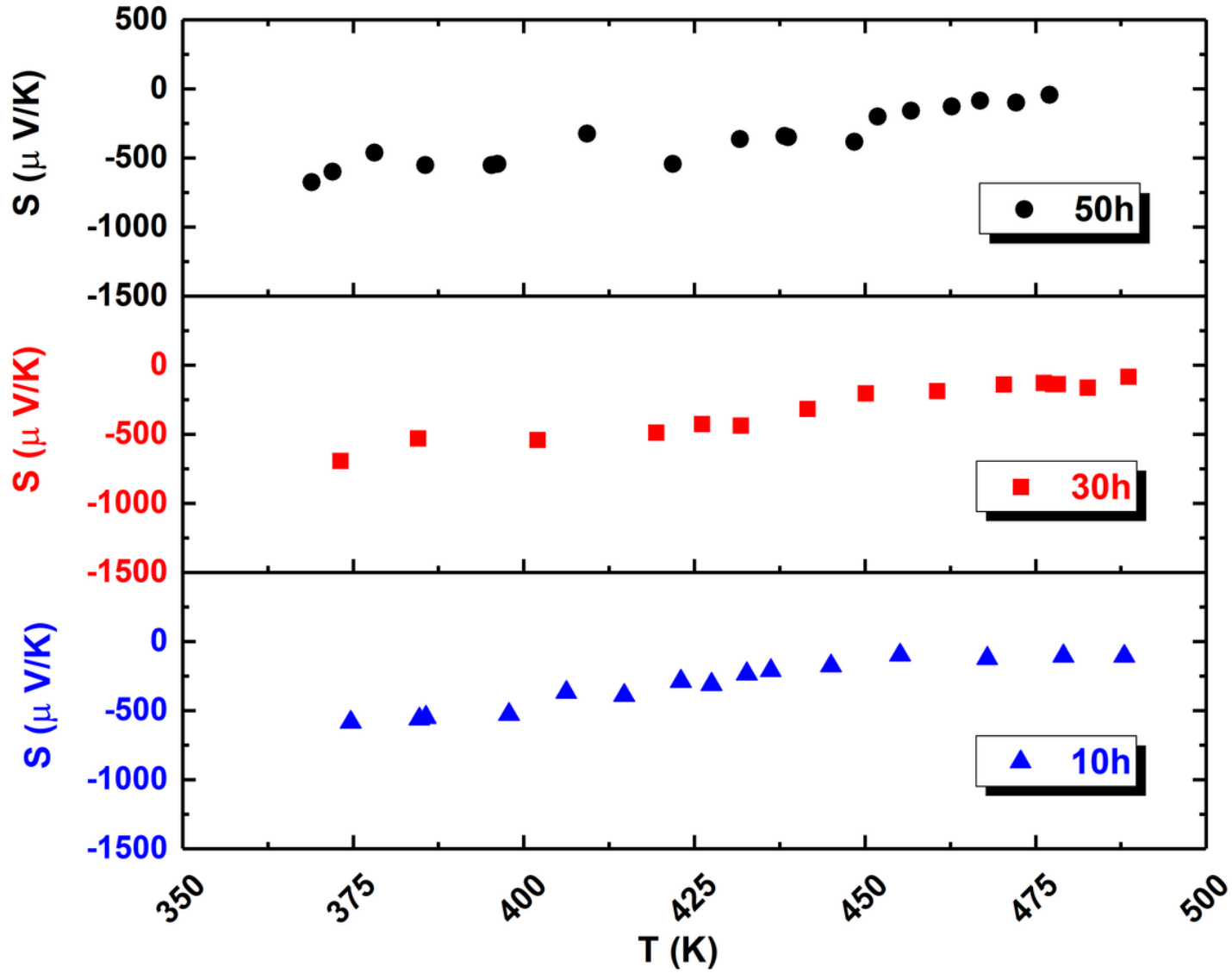

Figure 6

Seebeck coefficient of the sample at different milling time, 10h at (a), 30h at (b) and 50h at (c)

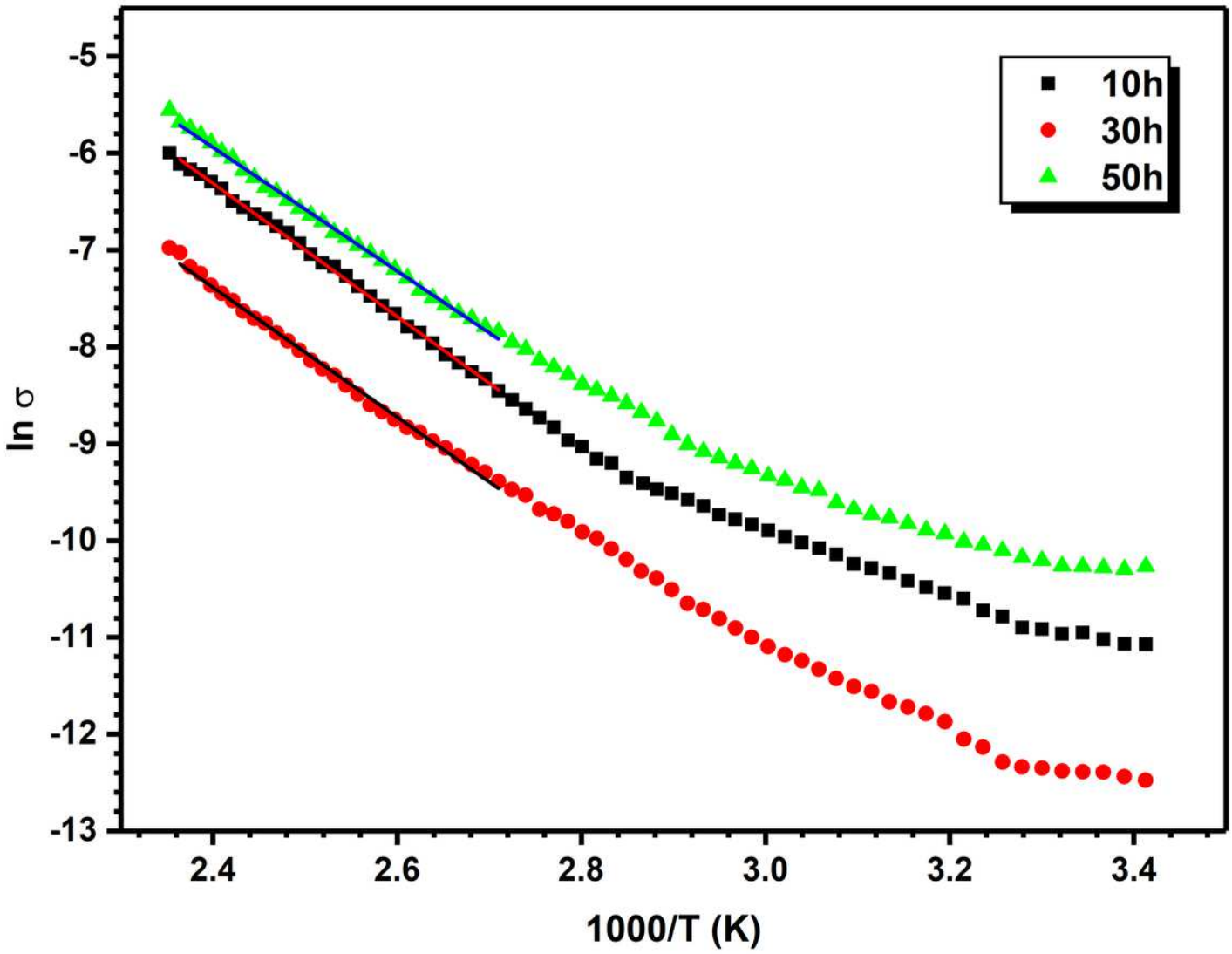

Figure 7

dc conductivity of ball milled MnO2 – Bi2O3 for different time heat-treated at 1073 K for five hours.

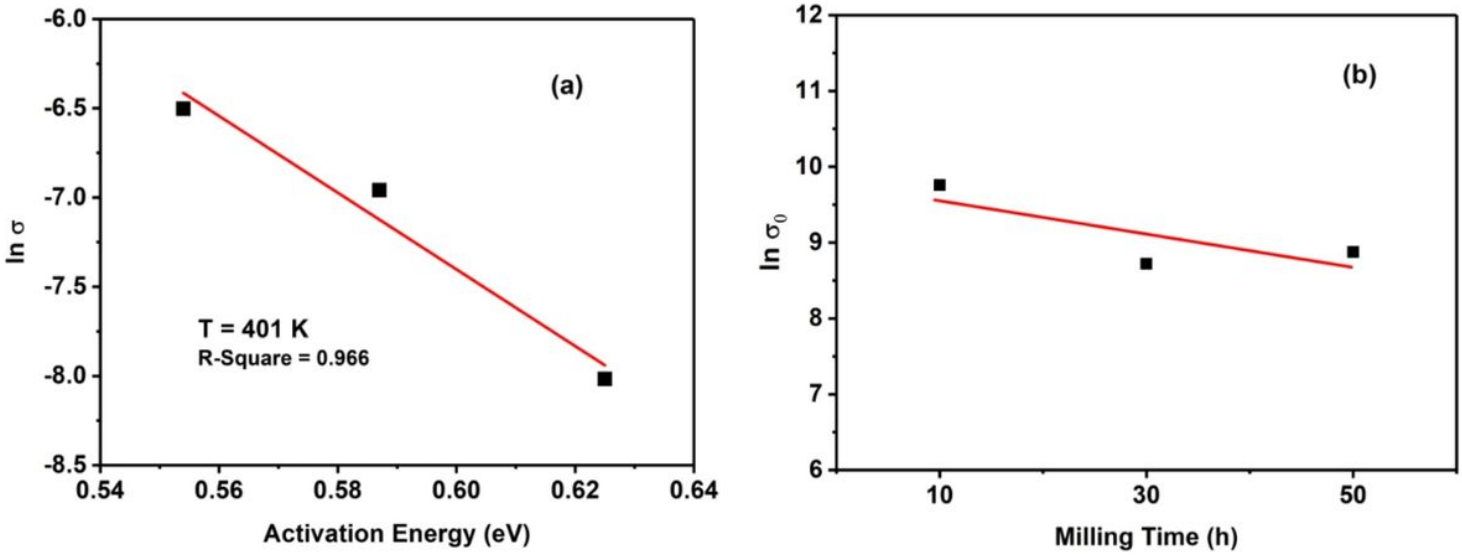

Figure 8

(a) samples logarithmic D.C conductivity variation with activation energy at 401K, (b) effect of milling time on the pre-exponential factors